Spatial Statistics 10 (2014) 76–86

Contents lists available at ScienceDirect

Spatial Statistics

journal homepage: www.elsevier.com/locate/spasta

Point-pattern analysis on the sphere

Scott M. Robeson [a,*], Ao Li [b], Chunfeng Huang [b]

[a] Departments of Geography and Statistics, Indiana University, Bloomington, IN 47405, USA
[b] Department of Statistics, Indiana University, Bloomington, IN 47408, USA

ARTICLE INFO

Article history:
Received 25 June 2014
Accepted 7 October 2014
Available online 16 October 2014

Keywords:
K-function
Spatial analysis
Global sampling networks
Spherical grids
Global change

ABSTRACT

Many important environmental, geographic, and geophysical variables are observed at the global scale, so it is important to extend point-pattern methods to the sphere. Here, we develop the *K* function on the sphere and then evaluate several global data structures and networks. The assumption of complete spatial randomness (CSR) gives a *K* function that is proportional to the square of distance in Euclidean space, but we find that CSR on the sphere is proportional to 1 − cos(angular distance). To evaluate the spherical *K* function, we analyze two global data structures: latitude-longitude and equidistant hexagonal grids. Due to over-representation of polar regions, latitude-longitude grids produce clustered point patterns. The hexagonal grid is equal-area on the sphere and produces a dispersed point pattern. We also analyze the structure of an observing system for global climate research that is intended to have relatively even spatial coverage. We find that, due to its coastal and continental biases, the climate-station network produces clustered point patterns over a range of distances. Our focus is on planetary-scale geographic point distributions, but we foresee applications of spherical *K* functions in disciplines such as astronomy, geodetics, anatomy, and neuroscience. Software for spherical point-pattern analysis is available from the authors.

* Correspondence to: 701 E Kirkwood Ave, 120 Student Building, Indiana University, Bloomington, IN 47405, USA. Tel.: +1 812 855 6303.
E-mail address: srobeson@indiana.edu (S.M. Robeson).

http://dx.doi.org/10.1016/j.spasta.2014.10.001
2211-6753/

1. Introduction

The study of point patterns has a long history and plays an important role in spatial analysis (Ripley, 1977; Getis, 1984; Upton and Fingleton, 1985; Diggle, 2003). Spatial point patterns can be characterized as ranging from dispersed to clustered, with random point patterns having elements of both dispersion and clustering (Fig. 1(a)–(c)). Characterizing spatial point patterns helps to understand the processes that generate the points. For instance, ecological processes related to reproductive success, abiotic factors, and competition can be inferred from the spatial arrangement of trees in a landscape. The locations of tree species may produce clustered patterns due to preference for certain climatic conditions while others may be dispersed due to competition or interactions with soil fungi (Legendre and Fortin, 1989; Packer and Clay, 2000). In addition to studying spatial processes, point-pattern analysis is also valuable for evaluating the efficacy of sampling networks, particularly those that are designed to be relatively dispersed or random.

In the past, quadrat- and nearest-neighbor-based methods have been used to explore point patterns and associated processes (e.g., Harvey, 1966; Clark and Evans, 1954). Both of those approaches have well-known limitations such as the scale problem for quadrat-based methods and a local bias for nearest-neighbor analysis (Burt et al., 2009). By far, the most widely used approach to the study of spatial point patterns is the K function or Ripley's K (Ripley, 1977, 2005), which allows a point pattern to be analyzed over a range of distances (Fig. 1(d)–(e)). A point-generating process, therefore, might be found to have a K function that shows clustering or dispersion over short distances but other patterns over longer distances. As a result, the K-function approach is flexible, easy to interpret, and Monte Carlo confidence intervals are straightforward to create using randomly generated point patterns. The confidence intervals typically are created on the assumption of complete spatial randomness (CSR), but other null models are sometimes used (Diggle, 2003). The K function can also be adjusted for edge effects near the boundaries of the study area where one encounters fewer points than expected (Yamada and Rogerson, 2003).

Nearly all formulations and applications of point-pattern analysis have been conducted in two-dimensional Euclidean space—that is, the plane. Many environmental, geographic, and geophysical variables that are observed or sampled at the global scale, however, are more appropriately studied on the sphere. Many spatial interpolation methods have been adapted for the spherical domain (Wahba, 1981; Renka, 1984; Willmott et al., 1985; Schaffrin, 1993; Robeson, 1997), but point-pattern methods using spherical geometry have not been widely studied and were only briefly mentioned in Ripley (1977). In this article, we extend the most widely used method of point-pattern analysis – Ripley's K function – to the sphere in order to analyze global-scale point patterns. After developing the mathematical basis for the K function on the sphere, we show the utility of the approach by analyzing two commonly used global data structures: a fixed latitude-longitude grid and an equidistant hexagonal grid. Finally, we analyze a set of upper-air climate stations to assess the attributes of an important global sampling network.

2. Theory

Spatial processes can have different characteristics when using Euclidean and spherical geometry. For example, some widely used covariance functions in Euclidean space have been shown to be invalid (not positive-definite) on the sphere (Huang et al., 2011; Gneiting, 2013). Although the Earth is more precisely described as an ellipsoid, nearly all types of spatial analysis at the global scale are well modeled using spherical geometry (Tobler, 2002; Schaffrin et al., 2003; Banerjee, 2005). While the characteristics of spatial point processes in Euclidean space have been studied extensively (e.g., Cressie, 1993; Diggle, 2003), we investigate spatial point processes on the sphere. Our approach here is analogous to that for Euclidean space presented by Diggle (2003).

For a spatial point process on the sphere $S^2(R)$ with radius R, we define both the first-order intensity (with $\mathrm{E}(\cdot)$ being expectation)

$$\lambda(p) = \lim_{|dp|\to 0}\left[\frac{\mathrm{E}\{N(dp)\}}{|dp|}\right],$$

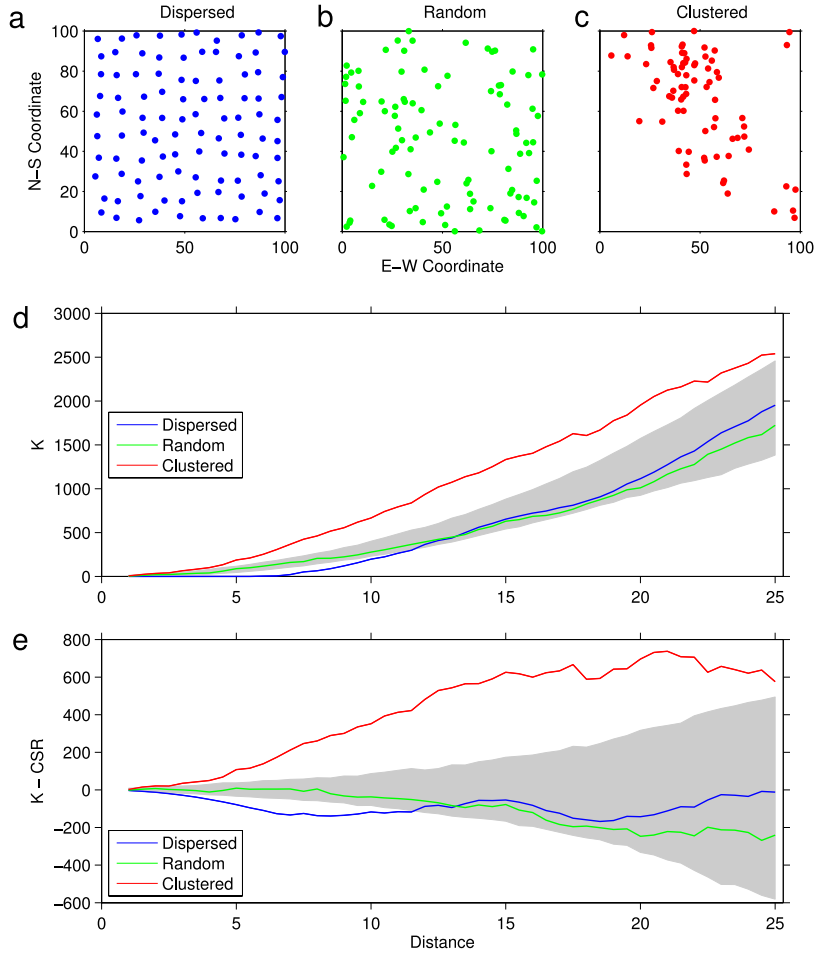

Fig. 1. Examples of (a) dispersed, (b) random, and (c) clustered point patterns in the plane, with their respective (d) K functions and (e) K functions with complete spatial random (CSR) model removed. Ninety-five percent confidence intervals for CSR are shown in (d) and (e). The formulation in (e) is convenient as values above zero represent clustered patterns while those below zero represent dispersed patterns.

and the second-order intensity

$$\lambda_2(p_1, p_2) = \lim_{|dp_1|,|dp_2|\to 0}\left[\frac{\mathrm{E}\{N(dp_1)N(dp_2)\}}{|dp_1|\cdot|dp_2|}\right],$$

where dp is the small spherical cap centered at the point p, $N(dp)$ is the number of events within dp, $|dp|$ is the surface area of this cap and $p, p_1, p_2 \in S^2(R)$. When the process is assumed to be stationary and isotropic, we have

$$\lambda(p) = \lambda, \qquad \lambda_2(p_1, p_2) = \lambda_2(R\theta(p_1, p_2)),$$

where $R\theta(p_1, p_2)$ is the great-circle distance between p_1 and p_2 on $S^2(R)$. In the literature, such an assumption is termed homogeneity or rotation invariance on the sphere.

The first-order intensity (λ) gives the expected density of events (in the number per unit area) while the second-order intensity reveals the expected spatial dependency of the process. In practice, Ripley's K function (Ripley, 1977) is often used, as the relationship between the K function and the second-order intensity for a stationary isotropic point process in Euclidean space has been well

Table 1
Comparison of K and second-order intensity functions using 2-D Euclidean and spherical geometry, where r and y represent either planar or great-circle distances and R is the radius of the sphere.

	Euclidean	Spherical, $S^2(R)$
K function in terms of λ_2	$K(r) = \frac{2\pi}{\lambda^2}\int_0^r \lambda_2(y)ydy$	$K(r) = \frac{2\pi R}{\lambda^2}\int_0^r \lambda_2(y)\sin(y/R)dy$
λ_2 in terms of K' function	$\lambda_2(r) = \lambda^2(2\pi r)^{-1}K'(r)$	$\lambda_2(r) = \lambda^2(2\pi R\sin(r/R))^{-1}K'(r)$
CSR	$K(r) = \pi r^2$	$K(r) = 2\pi R^2(1-\cos(r/R))$

documented (Ripley, 1977; Cressie, 1993; Diggle, 2003). We extend this connection to the spherical setting and define

$$\lambda K(r) = \mathrm{E}\{N_p(r)\},$$

where λ again is the first-order intensity on the sphere and $N_p(r)$ is the number of extra events on the spherical cap centered at p with arc to be r. When the process on the sphere is assumed to be stationary, isotropic, and orderly (Diggle, 2003, p. 44), we obtain the following:

$$K(r) = \frac{2\pi}{\lambda^2}\int_0^r \lambda_2(y)R\sin(y/R)dy, \tag{1}$$

where R is the radius of the sphere. This is analogous to, but mathematically different from its planar counterpart where

$$K(r) = \frac{2\pi}{\lambda^2}\int_0^r \lambda_2(y)ydy. \tag{2}$$

The difference between these two equations lies within the integrands where the annulus of width dy of radius y is considered. When the process is in two-dimensional Euclidean space, the annular area is given by $2\pi ydy$, while on the spherical surface the annular area is given by $2\pi R\sin(y/R)dy$.

As a quick reference, Table 1 provides an overview of the salient features of both cases. Note that if one replaces $\sin(y/R)$ by its first-order Taylor expansion y/R, the two K functions will yield exactly the same form. This indicates that when the dimensions of the study area are relatively small compared to the sphere's radius, the point process can be approximated by the planar form (and that the coordinates within an appropriate cartographic projection would be used in place of latitude and longitude). However, as one studies larger areas or the entire sphere, the approximation diverges and one should use the spherical form of the K function.

Eq. (1) shows the K function in terms of the second-order intensity function λ_2. Reversely, λ_2 can be expressed in terms of the K function through the derivative

$$\lambda_2(r) = \frac{\lambda^2}{2\pi R\sin(r/R)}K'(r).$$

Once again, this expression is analogous to its planar counterpart (see Table 1) and was briefly mentioned in Ripley (1977). If one further assumes complete spatial randomness (CSR) on the sphere, that is

$$\lambda(p) = \lambda, \qquad \lambda_2(r) = \lambda^2,$$

then the K function for CSR can also be obtained:

$$K(r) = \frac{2\pi}{\lambda^2}\int_0^r \lambda^2 R\sin(y/R)dy = 2\pi R^2(1-\cos(r/R)).$$

While it is clear that this form of CSR is different from its planar counterpart (Table 1), a straightforward comparison helps to determine the length scale at which the planar approximation begins to fail (Table 2 and Fig. 2). Using a radius for Earth of $R = 6371$ km, when distances in the K function extend beyond about 3000 km the planar approximation will begin to yield a nontrivial error and the spherical approach is recommended. Clearly, if the analysis is performed at the global scale, one should use the

Table 2
Example values of planar and spherical integrands of K function: r/R and $\sin(r/R)$, as well as example values of K-functions for CSR: $\pi(r/R)^2$ and $2\pi(1-\cos(r/R))$, where $R = 6371$ km. Here, great-circle distance (r) is used in both cases, so all differences are due to the planar approximation in the K function and do not include errors due to distance calculations.

	r/R	$\sin(r/R)$	$\pi(r/R)^2$	$2\pi(1-\cos(r/R))$
$r = 500$ km	0.0785	0.0784	0.0193	0.0193
$r = 1000$ km	0.1570	0.1563	0.0774	0.0772
$r = 2000$ km	0.3139	0.3088	0.3096	0.3071
$r = 3000$ km	0.4709	0.4537	0.6966	0.6838
$r = 4000$ km	0.6278	0.5874	1.2384	1.1982
$r = 5000$ km	0.7848	0.7067	1.9350	1.8377
$r = 10000$ km	1.5696	0.9999	7.7399	6.2757

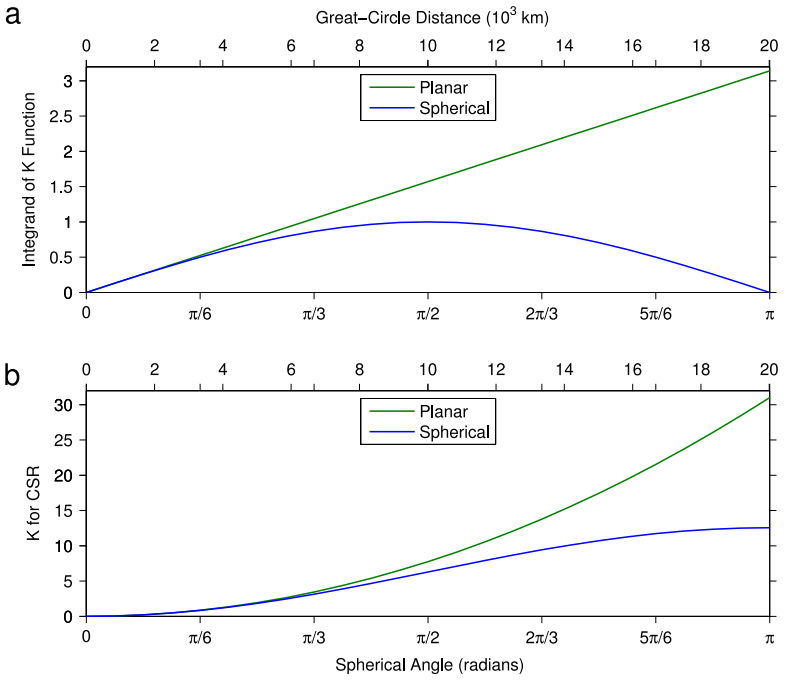

Fig. 2. Comparison of values of (a) the integrand of the K function and (b) CSR for K functions using planar (green line) and spherical geometry (blue line) as a function of distance (or spherical angle). The two begin to diverge at around $\pi/6$ radians or ≈ 3000 km.

spherical K function approach developed here. Like the simplistic estimation of great-circle distance using Euclidean approaches (Banerjee, 2005), the spherical K function terms in Table 2 and Fig. 2 are always overestimated when using the corresponding planar formulations. Note that, to isolate the error in using Euclidean approximations for the K function, we used great-circle distances for the planar representations (r/R and $\pi(r/R)^2$). As a result, all differences in Table 2 and Fig. 2 result from using planar approximations within the K function and are not due to errors from planar distance calculations.

To estimate the K function in practice, we use an approach similar to Diggle (2003, Eq. (4.14)). If one observes $\{p_1, \ldots, p_n\} \in S^2(R)$, we can estimate

$$\hat{K}(r) = \frac{4\pi R^2}{n(n-1)} \sum_{i=1}^{n} \sum_{j \neq i} I(R\theta(p_i, p_j) \leq r),$$

where $I(\cdot)$ is the indicator function. In Diggle (2003, Section 4.6) and Cressie (1993, Section 8.2.6), there is considerable discussion of the edge effects that arise when estimating the K function near the boundaries of a planar study area. Here, we note that if the point-generating phenomenon is truly a global scale, then one can estimate the K function on the sphere without considering edge effects.

3. Results and discussion

In this section, we analyze two important global data structures, a $10^\circ \times 10^\circ$ latitude-longitude grid and a hexagonal grid that is equal-area on the sphere. Finally, we analyze the point-pattern properties of the stations within an important sampling network for global climate monitoring. As with point-pattern studies in Euclidean space, visualization of the spatial distribution of points on the sphere is essential. For global-scale point patterns, we recommend an equal-area (or equivalent) map projection, such as the Mollweide projection. Random point patterns are likely to appear non-random when the map projection is not equivalent (Fig. 3). It should be noted, however, that no global-scale map can faithfully translate circles on the sphere to the mapped space, which makes the estimation of the K function for spherical data even more important than for planar data (where visualizations of point patterns provide more faithful representations).

3.1. Latitude-longitude grids

Fixed or "equally spaced" latitude-longitude grids are widely used for structuring global-scale data. Climate data sets and output from climate models, for instance, commonly use coarse resolution $5^\circ \times 5^\circ$ (Morice et al., 2012) or $2.5^\circ \times 2.5^\circ$ grids (Kistler et al., 2001). Finer resolution grids for climate data include analyses at resolutions of $0.5^\circ \times 0.5^\circ$ (Willmott and Robeson, 1995) and 30-arcsecond (0.083°; Daly et al., 2008). These grids are not equal-area and have a number of less-than-optimal properties (Goodchild and Shiren, 1992; White et al., 1992). Still, latitude-longitude grids continue to be the primary global data structure and even influence the perception and interpretation of global phenomena by overemphasizing polar regions relative to the tropics. It also can be argued that latitude-longitude grids have inadvertently caused the Plate Carée projection, which is neither equal-area nor conformal, to become the default map projection in many global change fora (e.g., Stocker et al., 2013). Here, we analyze the point-pattern properties of a $10^\circ \times 10^\circ$ grid, which contains a total of 18×36 or 648 nodes.

A $10^\circ \times 10^\circ$ latitude-longitude grid is somewhat coarse at the global scale, but still has a considerable number of points in polar regions (Fig. 4(a)). When naively viewed from the familiar Cartesian perspective – particularly within a Plate Carée projection – a fixed latitude-longitude grid might be expected to produce a dispersed point pattern. However, given the convergence of meridians towards the poles, latitude-longitude grids produce highly uneven representations of global-scale phenomena. The K function for the $10^\circ \times 10^\circ$ grid shows a distinct clustered pattern that extends to $\pi/2$ radians (Fig. 4(b)). While not unexpected, the highly clustered K function for the latitude-longitude grid clearly demonstrates the K-function's properties on the sphere, as well as the unusual characteristics of a ubiquitous spatial data structure.

Note that the K function is strictly positive, so the random point distributions that comprise the confidence intervals tend to produce a positively skewed distribution of K functions. As a result, the confidence-interval envelope tends to be slightly larger for positive values of $K -$ CSR than for negative ones.

3.2. Global hexagonal grids

While fixed latitude-longitude grids are the most widely used global data structure, tessellations of the sphere using the surfaces of regular polyhedra provide a more regular decomposition of the spherical surface. An example is the representation of the sphere using the icosahedron by partitioning into hexagonal grids that are equal area (e.g., Sahr et al., 2003). Here, we use the hexagonal tessellation at a resolution that produces 272 grid locations to evaluate the point-pattern properties of this unconventional but efficient spatial data structure. Sahr et al. (2003) refer to this grid as the

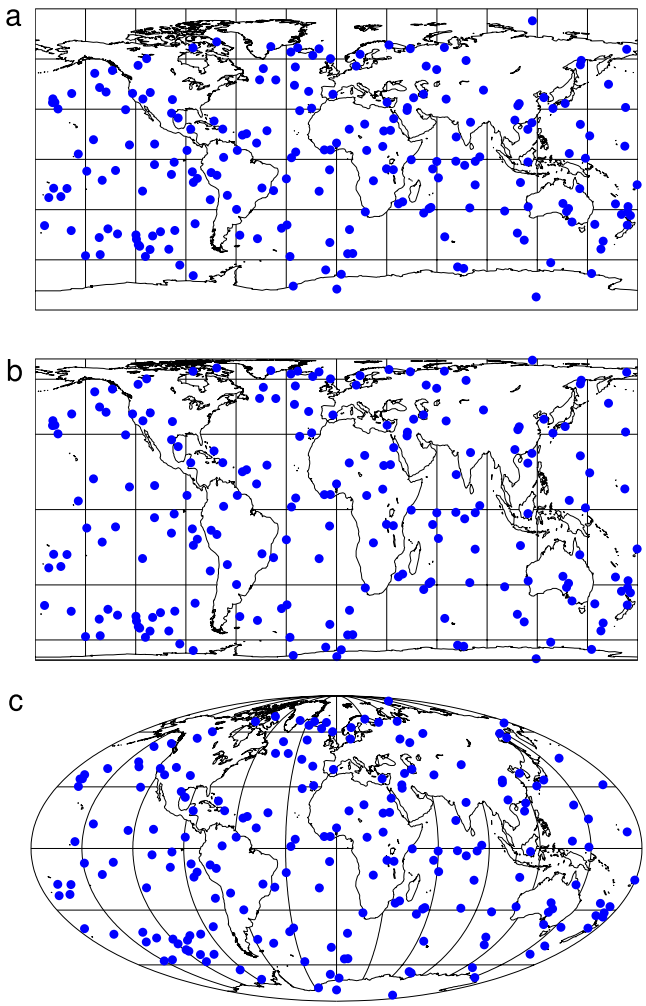

Fig. 3. Visual interpretation of global-scale point patterns is strongly influenced by choice of map projection. Here, 200 randomly generated points on the sphere are viewed in the: (a) Plate Carée projection, (b) equal-area Lambert's cylindrical projection, and (c) equal-area Mollweide projection. The Plate Carée, or plane chart, projection is not equal area and makes polar regions appear under-sampled. The two equal-area projections provide slightly different representations of the relative randomness of the point pattern, but the cylindrical projection inaccurately depicts the poles as lines.

Icosahedral Snyder Equal Area Aperture 3 Hexagon at resolution 3 (ISEA3H3). The centers of each of these hexagons are shown in an equal-area map projection and demonstrate an even distribution on the sphere (Fig. 5(a)). Note that other latitude-longitude systems including isothermal and authalic coordinates (Tobler and Chen, 1986; Schaffrin et al., 2003) have been discussed in the literature to achieve the equal-area map projection.

As an equal-area decomposition of the sphere, the hexagonal grid is expected to produce a well-dispersed point pattern. The K function for the hexagonal grid clearly shows its dispersed nature at angular distances up to $\pi/2$ radians (Fig. 5(b)). Here, we used an angular distance increment of 0.2 rad. With a finer choice for the distance increment, such as 0.1 rad, the K function for this grid produces an alternating dispersed-random pattern as the distance calculation hits each set of equidistant

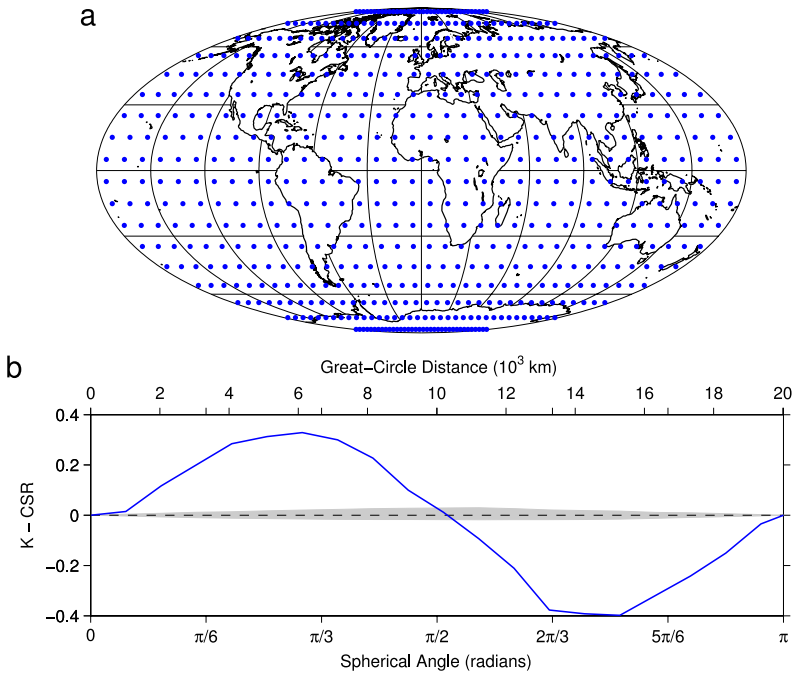

Fig. 4. Point patterns associated with a $10^\circ \times 10^\circ$ latitude-longitude grid: (a) equal-area map of the 648 points and (b) spherical K function (minus CSR) with 99% confidence intervals. The clustered pattern of latitude-longitude grids is clearly evident as an over-representation of polar regions in both the map and the K function. In this grid, a 10° grid box near the equator represents over 11 times as much area as does a 10° grid box near the poles.

neighbors on the hexagonal grid and suddenly pushes the K function to a higher value. As a result, careful selection of – and some experimentation with – the distance increment usually is warranted, particularly with patterns derived from nonrandom or relatively small sample sizes (here, $n = 272$).

3.3. Upper-atmosphere sampling network (GUAN)

Global-scale sampling networks have been created for many geophysical phenomena, such as those for monitoring atmospheric temperature, trace gases, oceanic salinity, gravity anomalies, and seismic variables. In most cases, the goal is to provide good coverage of the entire planet in terms of (i) the desired density of points and (ii) the relative evenness of the sample. As a result, from a point-pattern perspective, global sampling networks aim at having sufficient first- and second-order properties. Often, however, the sample size and a map are the only tools used to evaluate the sampling network's characteristics. Equal-area maps are essential to network evaluation, but we strongly recommend that the K function for global sampling networks also be a part of the evaluation process.

Many networks have been established under the Global Climate Observing System (GCOS, 2007), and one that is widely used in climate studies is the GCOS Upper-Air Network (GUAN). The GUAN is a planetary-scale distribution of 172 locations where weather-balloon data are regularly collected. GUAN data have been used to analyze a wide range of climate patterns and their trends, such as temperature and water-vapor variations in the troposphere and stratosphere (Allen and Sherwood, 2008; Thorne et al., 2005). Not all data are available for all time periods, but we use the full set of 172 GUAN stations to evaluate its "best-case" characteristics as a spherical point pattern.

The map of GUAN locations (Fig. 6(a)) shows a global sample that has good coverage but is somewhat biased towards continental and coastal locations. Understandably, large areas of the Pacific and Atlantic Oceans are relatively unsampled. Over relatively short spherical distances ($<$1000 km), the K function for the GUAN data shows a dispersed point pattern (Fig. 6(b)). This represents an

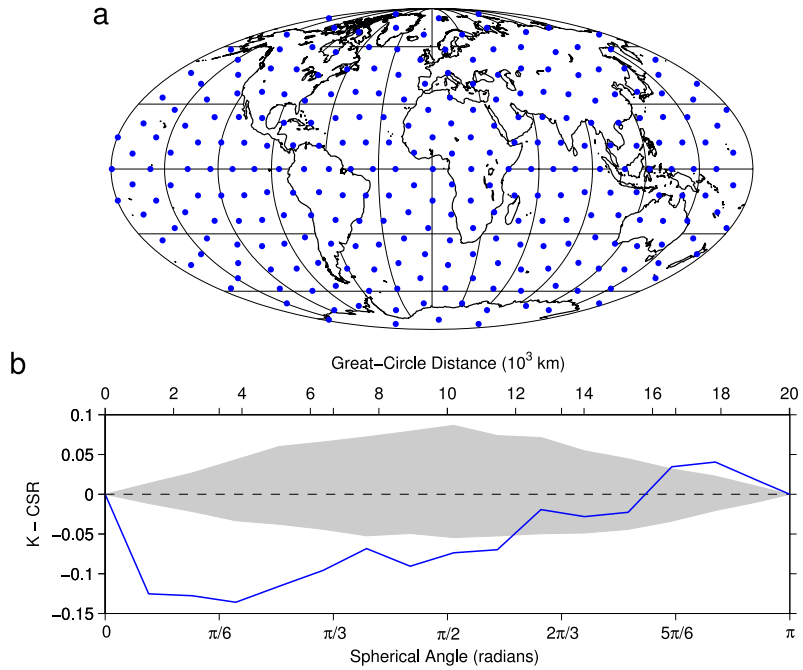

Fig. 5. Point patterns associated with a global hexagonal grid: (a) equal-area map of the 272 points and (b) spherical K function (minus CSR) with 95% confidence intervals. The grid clearly has a dispersed pattern in both the map and the K function.

acceptable inter-station distance for most upper-air variables, which have very long correlation distances (Julian and Thiébaux, 1975). Beyond those short distances and up to 5000 km, however, the spherical point distribution produces a clustered pattern. This indicates a sampling bias and potential shortcoming in the GUAN distribution. In selecting stations for the GUAN, it appears that there has been a desire to have locations that are more than about 1000 km apart and the network clearly shows dispersion below this distance. Beyond about 1500 km ($\pi/12$ rad), however, there is a tendency towards clustering with positive values of $K-$ CSR extending over most spherical distances. Overall, it appears that the addition of stations that have a more distinctive set of inter-station distances could improve the sampling characteristics and dispersion of the network.

4. Conclusions

While point-pattern analysis in the plane has been widely studied, here we analyze point patterns on the sphere. By summarizing the mathematical foundation for the spherical K function, we show that complete spatial randomness (CSR) is proportional to the $1-\cos(\text{angular distance})$ on the sphere. We then evaluated a fixed $10^\circ \times 10^\circ$ latitude-longitude grid to show that it produces sampling patterns that are highly clustered and overemphasize polar regions. In contrast, grids that are based on a hexagonal decomposition of the sphere have dispersed point patterns that illustrate their optimal sampling properties. Lastly, we evaluated an important sampling network used in the study of global climate data. The global sampling network (GUAN) was designed for (approximately) uniform spatial coverage of the planet, but its K function demonstrates that it is a clustered sample because of the limitations of placing stations in terrestrial locations. The methods developed here would be helpful in re-evaluating the GUAN's K function as new station locations are considered for addition. We also hope that the spherical version of the K function will find useful applications in the evaluation and design of other global sampling networks.

In planar point-pattern analysis, edge effects occur when a sample point is close to a boundary and the corresponding distance (circle) falls partially outside the study area. For spherical point patterns,

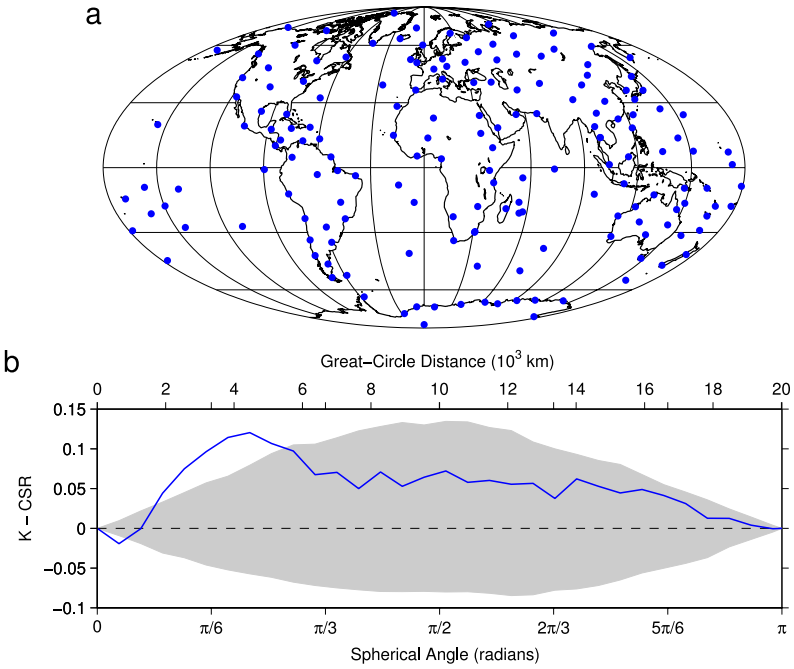

Fig. 6. Point patterns associated with a sampling network of 172 upper-air monitoring stations: (a) equal-area map of the station locations and (b) spherical K function (minus CSR) with 95% confidence intervals. Known as the GCOS upper-air network (GUAN), the network was created to have a relatively uniform sampling strategy but shows a dispersed K function only at very short distances. Due to a continental and coastal bias, the K function shows a clustered pattern over a wide range of important inter-station distances.

if the point-generating phenomenon is truly global – and being analyzed at that scale – then one can estimate the K function on the sphere without adjusting for edge effects. While this is an important feature of the K-function estimator on the sphere, it may be desirable in some instances to perform point-pattern analysis over a portion of the spherical surface, such as over a hemisphere, an ocean basin, or a continent. In those cases, edge-effect corrections analogous to those for the planar case need to be developed using spherical geometry.

Our focus here has been on global-scale geographic data and their point patterns, but there are many potential applications of spherical point-pattern analysis in other fields such as astronomy, geodetics, anatomy, and neuroscience. In addition, extensions of this work to account for non-accumulative point-pattern analysis, such as a spherical O-ring statistic, and multivariate point patterns are fruitful areas for future studies. Software (MATLAB functions and an R package) for K-function analysis on the sphere is available from the authors.

Acknowledgments

The authors would like to thank two anonymous reviewers for their insightful comments on an earlier version of this work. This research was supported in part by the US National Science Foundation (grant number 1208853) and by sabbatical leaves to S.R. and C.H. from Indiana University.

References

Allen, R.J., Sherwood, S.C., 2008. Warming maximum in the tropical upper troposphere deduced from thermal winds. Nat. Geosci. 1, 399–403.
Banerjee, S., 2005. On geodetic distance computations in spatial modeling. Biometrics 61, 617–625.
Burt, J.E., Barber, G.M., Rigby, D.L., 2009. Elementary Statistics for Geographers. Guilford Press, New York.

Clark, P.J., Evans, F.C., 1954. Distance to nearest neighbor as a measure of spatial relationships in populations. Ecology 35, 445–453.
Cressie, N., 1993. Statistics for Spatial Data. Wiley, New York.
Daly, C., Halbleib, M., Smith, J.I., Gibson, W.P., Doggett, M.K., Taylor, G.H., Curtis, J., Pasteris, P.P., 2008. Physiographically sensitive mapping of climatological temperature and precipitation across the conterminous United States. Int. J. Climatol. 28, 2031–2064.
Diggle, P.J., 2003. Statistical Analysis of Spatial Point Patterns, second ed. Academic Press, London.
GCOS, 2007. GCOS Upper-Air Network (GUAN): Justification, Requirements, Siting and Instrument Options. GCOS-112, WMO-TD 1379.
Getis, A., 1984. Interaction modeling using second-order analysis. Environ. Plann. A 16, 173–183.
Gneiting, T., 2013. Strictly and non-strictly positive definite functions on spheres. Bernoulli 19 (4), 1327–1349.
Goodchild, M.F., Shiren, Y., 1992. A hierarchical spatial data structure for global geographic information systems. CVGIP, Graph. Models Image Process. 54 (1), 31–44.
Harvey, D.W., 1966. Geographical processes and the analysis of point patterns: testing models of diffusion by quadrat sampling. Trans. Inst. Brit. Geogr. 40, 81–95.
Huang, C., Zhang, H., Robeson, S.M., 2011. On the validity of commonly used covariance and variogram functions on the sphere. Math. Geosci. 43, 721–733.
Julian, P.R., Thiébaux, H.J., 1975. On some properties of correlation functions used in optimum interpolation schemes. Mon. Weather Rev. 103 (7), 605–616.
Kistler, R., Collins, W., Saha, S., White, G., Woollen, J., Kalnay, E., Fiorino, M., 2001. The NCEP-NCAR 50-year reanalysis: monthly means CD-ROM and documentation. Bull. Am. Meteorol. Soc. 82 (2), 247–267.
Legendre, P., Fortin, M.J., 1989. Spatial pattern and ecological analysis. Vegetation 80 (2), 107–138.
Morice, C.P., Kennedy, J.J., Rayner, N.A., Jones, P.D., 2012. Quantifying uncertainties in global and regional temperature change using an ensemble of observational estimates: the HadCRUT4 data set. J. Geophys. Res. 117, D08101. http://dx.doi.org/10.1029/2011JD017187.
Packer, A., Clay, K., 2000. Soil pathogens and spatial patterns of seedling mortality in a temperate tree. Nature 404, 278–281.
Renka, R.J., 1984. Interpolation of data on the surface of a sphere. ACM Trans. Math. Software 10 (4), 417–436.
Ripley, B.D., 1977. Modelling spatial patterns. J. R. Stat. Soc. Ser. B 172–212.
Ripley, B.D., 2005. Spatial Statistics, Vol. 575. John Wiley & Sons, New York.
Robeson, S.M., 1997. Spherical methods for spatial interpolation: review and evaluation. Cart. Geog. Info. Sys. 24, 3–20.
Sahr, K., White, D., Kimerling, A.J., 2003. Geodesic discrete global grid systems. Cart. Geog. Info. Sci. 30, 121–134.
Schaffrin, B., 1993. Biased kriging on the sphere? In: Soares, A. (Ed.), Geostatistics Tróia'92, Vol. 5. Kluwer, Dordrecht, pp. 121–131.
Schaffrin, B., Mautz, R., Chum, C., Tseng, H., 2003. Toward a spherical pseudo-wavelet basis for geodetic applications. Comput.-Aided Civ. Infrastruct. Eng. 18, 369–378.
Stocker, T.F., et al. (Eds.), 2013. Climate Change 2013: The Physical Science Basis. Contribution of Working Group I to the Fifth Assessment Report of the Intergovernmental Panel on Climate Change. Cambridge University Press, Cambridge, UK.
Thorne, P.W., Parker, D.E., Tett, S.F., Jones, P.D., McCarthy, M., Coleman, H., Brohan, P., 2005. Revisiting radiosonde upper air temperatures from 1958 to 2002. J. Geophys. Res. 110, D18105. http://dx.doi.org/10.1029/2004JD005753.
Tobler, W., 2002. Global spatial analysis. Comput. Environ. Urban Syst. 26, 493–500.
Tobler, W., Chen, Z.T., 1986. A quadtree for global information storage. Geogr. Anal. 18 (4), 360–371.
Upton, G., Fingleton, B., 1985. Spatial Data Analysis by Example. Volume 1: Point Pattern and Quantitative Data. John Wiley & Sons, New York.
Wahba, G., 1981. Spline interpolation and smoothing on the sphere. SIAM J. Sci. Stat. Comput. 2, 5–16.
White, D., Kimerling, J.A., Overton, S.W., 1992. Cartographic and geometric components of a global sampling design for environmental monitoring. Cart. Geog. Info. Sys. 19 (1), 5–22.
Willmott, C.J., Robeson, S.M., 1995. Climatologically aided interpolation (CAI) of terrestrial air temperature. Int. J. Climatol. 15, 221–229.
Willmott, C.J., Rowe, C.M., Philpot, W.D., 1985. Small-scale climate maps: a sensitivity analysis of some common assumptions associated with grid-point interpolation and contouring. Amer. Cartog. 12, 5–16.
Yamada, I., Rogerson, P.A., 2003. An empirical comparison of edge effect correction methods applied to *K*-function analysis. Geogr. Anal. 37, 95–109.